Electronic Supplementary Information

Exploring Dual-Emission Properties in Mn^{4+} Distinctively Activated BaTaF$_7$ Red Emitting Phosphor

Konglan Chen [a], Shiyu Jia [a], Zifan Shao [a], Xinxin Han [b], Jian Yuan[a], Yayun Zhou [a*], Tingting Deng [a*]

[a] Guangdong-Hong Kong-Macao Joint Laboratory for Intelligent Micro-Nano Optoelectronic Technology, School of Physics and Optoelectronic Engineering, Foshan University, Foshan 528225, China

[b] School of Physical Science and Technology, MOE Key Laboratory of New Processing Technology for Non-ferrous Metals and Materials, Guangxi Key Laboratory of Processing for Non-ferrous Metals and Featured Materials, School of Resources, Environments and Materials, Guangxi University, Nanning 530004, China.

Corresponding author:

E-mail: zhou-yayun@foxmail.com (Y.Y. Zhou), tingtingdeng0803@163.com (T. T. Deng);
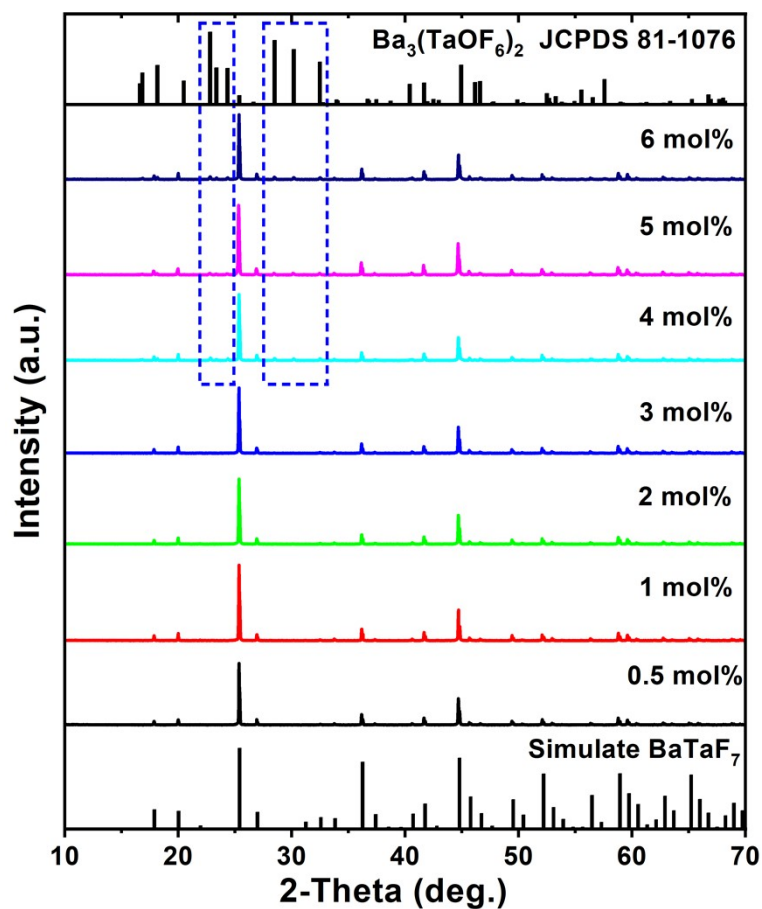
Figures

Fig. S1. X-ray diffraction patterns of BTF with different dopant

concentrations from 0.5 mol% to 6 mol%.
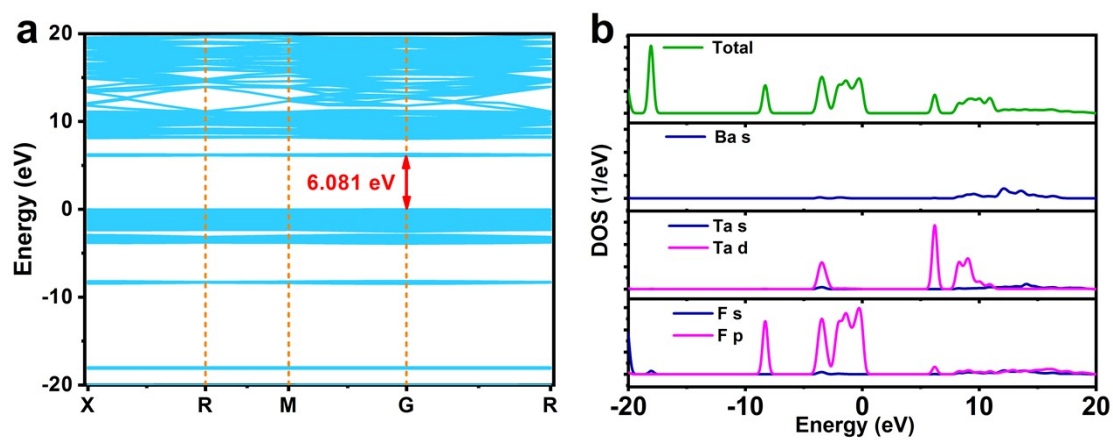

Fig. S2. The local symmetry of Mn^{4+} in $BaTaF_7$ was obtained after the M3,
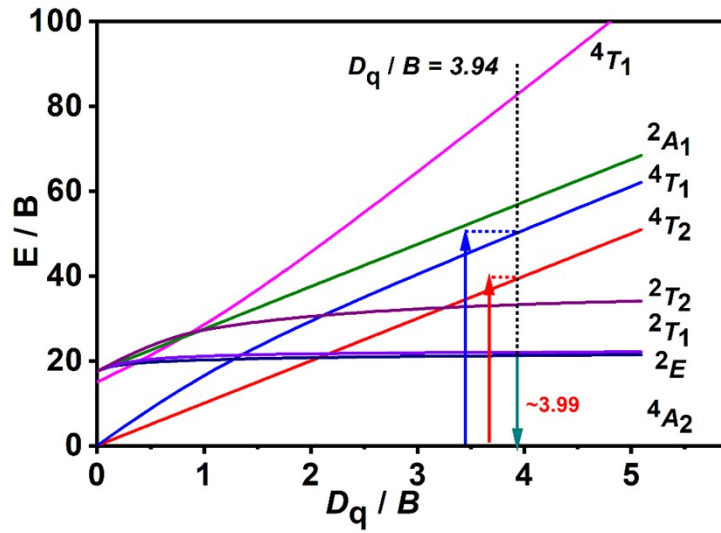
M4 and M5 models were optimized.

Fig. S3. Tanabe-Sugano energy-level diagram of Mn^{4+} ions in an
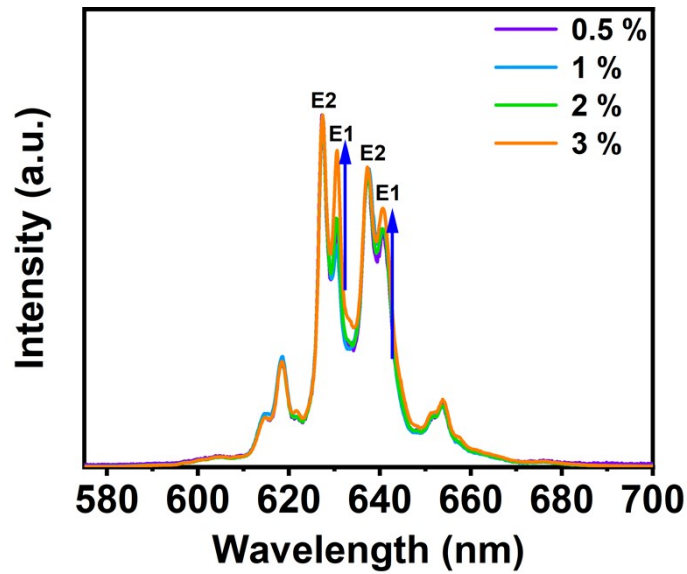
octahedral crystal field;

Fig.S4. Normalized PL spectra of BTF phosphors with different Mn^{4+}

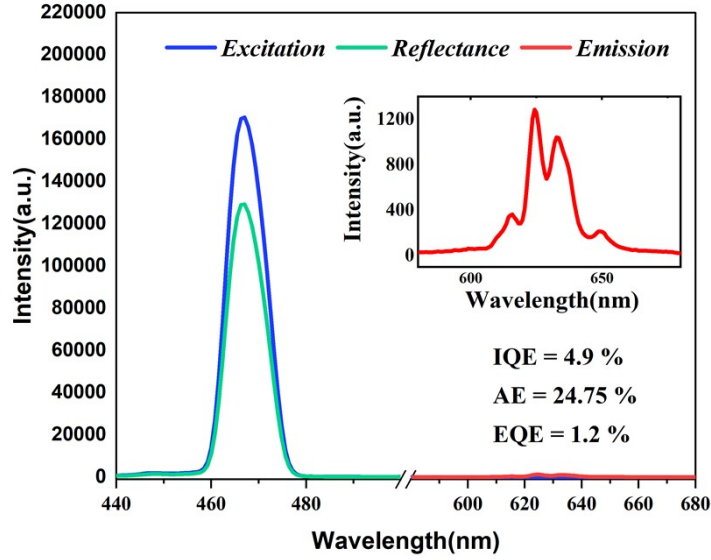doping concentrations.

Fig. S5. PL spectra of BTF(3%) and the reference sample measured using an integrating sphere for IQE, AE and EQE.

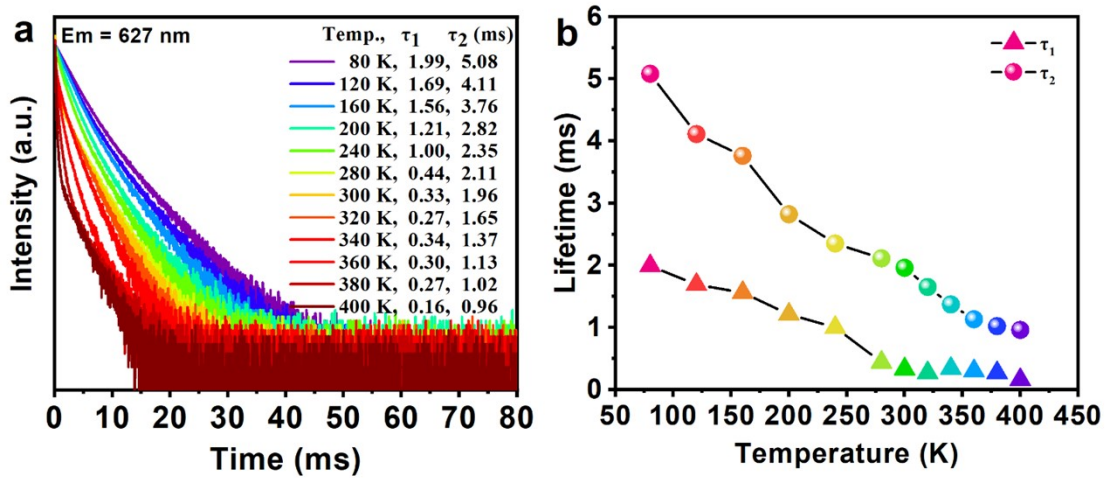**Fig. S6**. Temperature-dependent decay curves and lifetime analysis of $BaTaF_7$:3%Mn^{4+}. (a) Decay curves at 627 nm with increasing temperature. (b) Bi-exponential fitting of the decay curves to extract the lifetimes τ_1 and τ_2 at 627 nm.
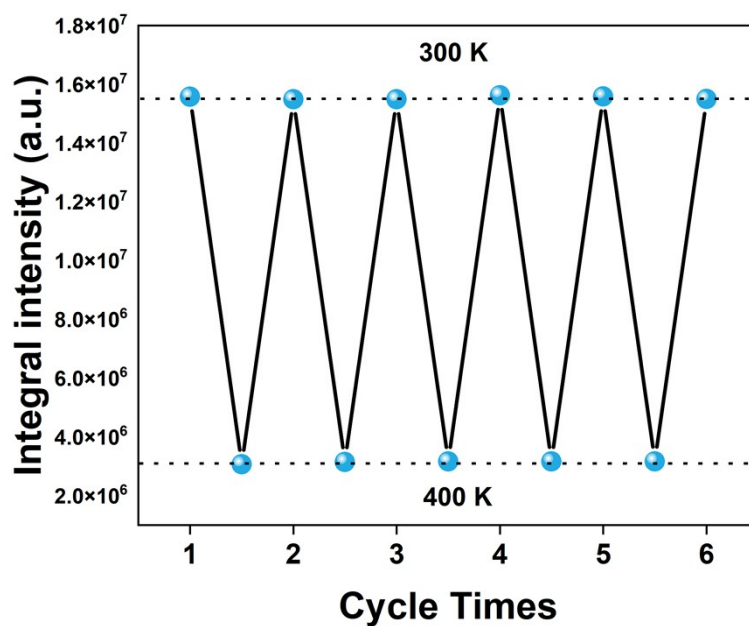
Fig. S7 PL integrated intensity of BTF (3%) at 300 K and 400 K during heating-cooling cycles.

Tables

Table S1 Schemes of different ratios of K_2MnF_6 to Ta_2O_5 for the experimental of $BaTaF_7:Mn^{4+}$ phosphor and actual doping amount of Mn^{4+} from ICP test results.

Sample	Experimental ratio of K_2MnF_6 to $BaTaF_7$ (mol %)	Actual doping concentration of Mn to Ta (mol %)
1	0.5	0.19
2	1	0.46
3	2	0.86
4	3	1.22
5	4	1.51

Table S2. The Refined structure parameters of $BaTaF_7:Mn^{4+}$ sample.

Atom	X	Y	Z	Occ.	B	Site
Ta	0.22374	0.22374	0.22374	0.9975	0.200	8c
Mn1	0.22374	0.22374	0.22374	0.0025	0.200	8c
Ba 1	0.00000	0.00000	0.00000	0.9975	0.518	4a
Mn2	0.00000	0.00000	0.00000	0.0025	0.518	4a

Ba 2	0.50000	0.00000	0.00000	1.000	0.722	4b
F 1	0.25800	0.05590	0.11680	1.000	0.200	24d
F 2	0.36420	0.27910	0.10250	1.000	0.200	24d
F 3	0.33590	0.33590	0.33590	1.000	1.650	8c

Table S3. Crystallographic data of $BaTaF_7$:Mn^{4+} (derived from the Rietveld structure analysis of XRD pattern)

Formula	$BaTaF_7 : Mn^{4+}$
Crystal system	Cubic
Space group	$Pa\bar{3}$
a (Å)	9.92864(6)
b (Å)	9.92864(6)
c (Å)	9.92864(6)
α	90.0000
β	90.0000
γ	90.0000
V_{cell} (Å^3)	978.744794(168)
Z	4
R_{wp}	8.318 %
R_p	6.590%
Gof	1.845

Table S4. The calculated formation energy (Ef) for four possible charge compensation models of Mn^{4+} in $BaTaF_7$.

Model	Compounds	Replacement forms	Defects	Formation energy (eV)
M1	$BaTaF_7$	$Mn^{4+} \rightarrow Ta^{5+}$ $Mn^{4+} \rightarrow Ba^{2+}$	F_i	7.05
M2	$BaTaF_7$	$Mn^{4+} \rightarrow Ta^{5+}$ $Mn^{4+} \rightarrow Ba^{2+}$	F_i	9.47
M3	$BaTaF_7$	$Mn^{4+} \rightarrow Ta^{5+}$	V_{F^-}	11.93
M4	$BaTaF_7$	$Mn^{4+} \rightarrow Ba^{2+}$	$V_{Ba^{2+}}$	21.02
M5	$BaTaF_7$	$2Mn^{4+} \rightarrow 2Ta^{5+}$ $Mn^{4+} \rightarrow Ba^{2+}$	/	27.61